



Development and verification of a hypoxia- and immune-associated prognosis signature for esophageal squamous cell carcinoma

Lian Lian^{1#}, Shi-Bing Teng^{2#}, You-You Xia^{3#}, Xiao-Ming Shen¹, Yan Zheng¹, Shu-Guang Han⁴, Wen-Jie Wang⁵, Xue-Fei Xu⁴, Chong Zhou⁶

¹Department of Oncology, Suzhou Xiangcheng People's Hospital, Suzhou, China; ²Department of Thoracic Surgery, Suzhou Xiangcheng People's Hospital, Suzhou, China; ³Department of Radiation Oncology, The Affiliated Lianyungang Hospital of Xuzhou Medical University (The First People's Hospital of Lianyungang), Lianyungang, China; ⁴Department of General Surgery, Suzhou Xiangcheng People's Hospital, Suzhou, China; ⁵Department of Radio-Oncology, The Affiliated Suzhou Hospital of Nanjing Medical University, Suzhou, China ⁶Department of Radiation Oncology, Xuzhou Central Hospital, Xuzhou, China

Contributions: (I) Conception and design: L Lian, YY Xia, XF Xu, WJ Wang, C Zhou; (II) Administrative support: XF Xu; (III) Provision of study materials or patients: L Lian, SB Teng, XM Shen, Y Zheng, SG Han, YY Xia, C Zhou; (IV) Collection and assembly of data: L Lian, SB Teng, XM Shen, YY Xia, SG Han; (V) Data analysis and interpretation: L Lian, WJ Wang, C Zhou; (VI) Manuscript writing: All authors; (VII) Final approval of manuscript: All authors.

[#]These authors contributed equally to this work.

Correspondence to: Chong Zhou. Department of Radiation Oncology, Xuzhou Central Hospital, Xuzhou 221009, China.

Email: zhouchongsuda@gmail.com; Wen-Jie Wang. Department of Radio-Oncology, The Affiliated Suzhou Hospital of Nanjing Medical University, Suzhou 215001, China. Email: suda_wangwenjie@163.com; Xue-Fei Xu. Department of General Surgery, Suzhou Xiangcheng People's Hospital, Suzhou 215131, China. Email: dr_xuxf@163.com.

Background: Esophageal cancer is one of the most common gastrointestinal malignancies worldwide, with high morbidity and mortality in China. The clinical importance of the interaction between hypoxia and immune status in the tumor microenvironment has been established in esophageal squamous cell carcinoma (ESCC). This study aims to develop a new hypoxia- and immune-based gene signature to predict the survival of ESCC patients.

Methods: The RNA-sequencing and clinical data of 173 cases of ESCC and 271 normal tissues were obtained from The Cancer Genome Atlas (TCGA) data portal and the Genotype-Tissue Expression (GTEx) database. Hypoxia-related genes (HRGs) and immune-related genes (IRGs) were retrieved from publicly shared data. Differentially expressed gene (DEG) analyses were carried out by the DESeq2 method using the edgeR package in R. Based on the intersection of the DEGs and HRGs/IRGs, differentially expressed HRGs (DEHRGs) and differentially expressed IRGs (DEIRGs) were obtained. DEHRGs and DEIRGs associated with prognosis were evaluated using univariate Cox proportional hazards analysis. A prognostic risk score model was constructed according to the genes acquired through Cox regression. Univariate analysis and Cox proportional hazards analysis were used to determine the independent prognostic factors related to prognosis. A nomogram was developed to predict the 1-, 2-, and 3-year overall survival (OS) probability.

Results: A total of 73 intersecting genes were obtained as DEHRGs and a total of 548 intersecting genes were obtained as DEIRGs. The risk score was established using 8 genes (*FABP7*, *TLR1*, *SYTL1*, *APLN*, *OSM*, *EGFR*, *IL17RD*, *MYH9*) acquired from univariate Cox analysis. Based on this 8-gene-based risk score, a risk prognosis classifier was constructed to classify the samples into high- and low-risk groups according to the median risk score. The nomogram model was constructed to predict the OS of ESCC patients.

Conclusions: The hypoxia- and immune-based gene signature might serve as a prognostic classifier for clinical decision-making regarding individualized management, follow-up plans, and treatment strategies for ESCC patients.

Keywords: Esophageal cancer; microenvironment; hypoxia; immune; prognosis

Submitted Dec 29, 2021. Accepted for publication Mar 08, 2022.

doi: 10.21037/jgo-22-69

View this article at: <https://dx.doi.org/10.21037/jgo-22-69>

Introduction

Esophageal cancer is one of the most common gastrointestinal malignancies worldwide, with high morbidity and mortality in China (1). Despite the rapid development of multidisciplinary therapies in recent years, the prognosis of esophageal cancer patients is still unsatisfactory (2). Esophageal squamous cell carcinoma (ESCC) and esophageal adenocarcinoma (EAC) are the predominant histological subtypes of esophageal cancer (3). In contrast to western countries, ESCC accounts for approximately 90% of all esophageal cancers in China, and is characterized by rapid progression and poor prognosis.

Hypoxia promotes ESCC progression and metastasis by accelerating tumor angiogenesis and stimulating tumor glycolysis (4,5). Hypoxic environment is significantly related to the poor prognosis in patients with ESCC (6). In addition, hypoxia plays an important role in promoting tumor immunosuppression and immune escape (7). Immune cells including cytotoxic T cells, natural killer cells (NK cells), regulatory T cells (Tregs), activated macrophages, and dendritic cells form the tumor microenvironment (TME) and are involved in the processes of tumor invasion, metastasis, and anti-tumor immune responses (8,9). There is a direct and indirect interaction between hypoxia and immune status in the TME of ESCC (10,11). Nevertheless, the molecular characteristics and mechanisms have not yet been clarified.

Tan *et al.* (12). revealed that hypoxia is correlated with prognosis and the incidence of immune cell infiltration in patients with esophageal cancer. Our study aimed to develop a prognostic signature composed of hypoxia- and immune-associated genes. Furthermore, we analyzed the correlation between the model and many kinds of infiltrating immune cells. Based on these, we constructed a nomogram model to predict the overall survival (OS) of ESCC patients by integrating the risk score and well-known prognostic factors, with an aim to improve the prognosis of ESCC. We present the following article in accordance with the TRIPOD reporting checklist (available at <https://jgo.amegroups.com/article/view/10.21037/jgo-22-69/rc>).

Methods

Patients

The RNA-sequencing and clinical data of 173 cases of ESCC and 271 normal tissue samples were obtained from The Cancer Genome Atlas (TCGA) data portal (https://xenabrowser.net/datapages/?dataset=TCGA-ESCA.htseq_counts.tsv&host=https%3A%2F%2Fgdc.xenahubs.net&removeHub=https%3A%2F%2Fxcna.treehouse.gi.ucsc.edu%3A443) and the Genotype-Tissue Expression (GTEx) database (https://xenabrowser.net/datapages/?dataset=gtex_RSEM_Hugo_norm_count&host=https%3A%2F%2Ftoil.xenahubs.net&removeHub=http%3A%2F%2F127.0.0.1%3A7222). Then, we combined the 2 sets of samples and performed batch processing on the training set data for analysis. The study was conducted in accordance the Helsinki Declaration (as revised in 2013).

Hypoxia-related genes (HRGs) and immune-related genes (IRGs)

The HRGs list containing 200 genes was downloaded from https://www.gsea-msigdb.org/gsea/msigdb/cards/HALLMARK_HYPOXIA (Table S1). The IRGs list consisting of 1793 genes was retrieved from ImmPort Shared Data (<https://immport.org/shared/home>), which shares basic cancer immunological data. The IRGs list is shown in the additional file, website: <https://cdn.amegroups.com/static/public/jgo-22-69-1.pdf>.

Identification of differentially expressed genes (DEGs), differentially expressed HRGs (DEHRGs), and differentially expressed IRGs (DEIRGs)

DEG analyses were carried out by the DESeq2 method using the edgeR package in the R statistical environment (<http://bioconductor.org/packages/edgeR/>) (R Development Core Team, Vienna, Austria). A total of 6299 DEGs, including 2164 up-regulated genes and 4135 down-regulated genes, were obtained (with the thresholds of $|\log_2$ fold change (FC)| >2.0 and adjusted P < 0.05), and

the heat map and volcano plot were generated. Based on the intersection of the DEGs and HRGs, 73 genes were obtained as DEHRGs. Similarly, DEIRGs were obtained by intersecting DEGs with IRGs.

Functional enrichment analysis

According to the mRNA expression of the DEHRGs and DEIRGs, Gene Ontology (GO) and Kyoto Encyclopedia of Genes and Genomes (KEGG) enrichment analysis were performed using the R package Cluster Profiler. GO annotation and KEGG pathways were plotted using the GPlot package in R.

Development of a risk score model and validation model

DEHRGs and DEIRGs associated with prognosis were evaluated using univariate Cox proportional hazards analysis. The genes with prognostic significance were selected with $P < 0.05$ as the threshold and the results were illustrated in a forest plot. Then, the least absolute shrinkage and selection operator (LASSO) method (13) was performed for dimensionality reduction filtering using the glmnet package of R. Redundant factors were removed and corresponding genes were selected. In addition, a prognostic risk score model was constructed according to the genes acquired through Cox regression.

$$\text{Risk Score}(RS) = \sum_{i=1}^n (\text{Coef}_i \times X_i) \quad [1]$$

In this formula, *Coef_i* is the risk coefficient of signature genes and *X_i* indicates the identified genes. *Coef_i* was obtained from Cox analysis. Based on the individual risk scores, the samples were classified into high-risk and low-risk categories using the median risk score as the cut-off, and survival curves were plotted using Kaplan-Meier (KM) analysis. In order to verify the stability of the model, subgroup survival curves were generated based on the high- and low-risk groups combined with clinical variables [including smoking status, body mass index (BMI), radiotherapy status, TNM stage, and gender].

Analysis of the relationship between the risk score model and immune cell infiltration

The relative ratios of 22 infiltrating immune cell types in the specimens were calculated by using the CIBERSORT

software (14). CIBERSORT is a deconvolution algorithm that uses a set of reference gene expression values (547 genes) to predict the proportions of 22 infiltrating immune cell types from sample expression data by using support vector regression. The association between the risk score model and immune cell infiltration was analyzed.

Development and evaluation of the nomogram

Univariate analysis and Cox proportional hazards analysis were used to determine the independent prognostic factors related to prognosis, including the risk score model and clinicopathological characteristics of the patients. The nomograms were developed to predict the 1-, 2-, and 3-year OS probability (15,16). A calibration curve was drawn to determine the divergence between the nomogram's predicted probability and the actual incidence. A calibration curve was drawn to define the discrepancy between the predicted probability of the nomogram and the actual incidence.

Statistical analysis

All statistical analyses were carried out using R software v3.5.2. Independent prognostic factors were determined by using a multivariate Cox regression model. Patient survival time was analyzed using KM curves, and the log-rank test was used for statistical analysis. The area under the curve (AUC) of the survival receiver operating characteristic (ROC) curve was calculated via the survival ROC R software package to validate the performance of the prognostic signature (16). $P < 0.05$ was considered to indicate a statistically significant difference.

Results

Identification DEGs, DEIRGs, and DEHRGs

DEG analysis was carried out using the DESeq2 method. A total of 6,299 DEGs were obtained, including 2,164 up-regulated and 4,135 down-regulated genes (based on log₂ FC). The heat map and volcano plot were drawn as shown in Figure 1A,1B. The DEGs and 200 HRGs were intersected, and 73 intersection genes were obtained as DEIRGs (Figure 1C). The DEGs and known IRGs were intersected, and 548 intersection genes were obtained as DEHRGs (Figure 1D).

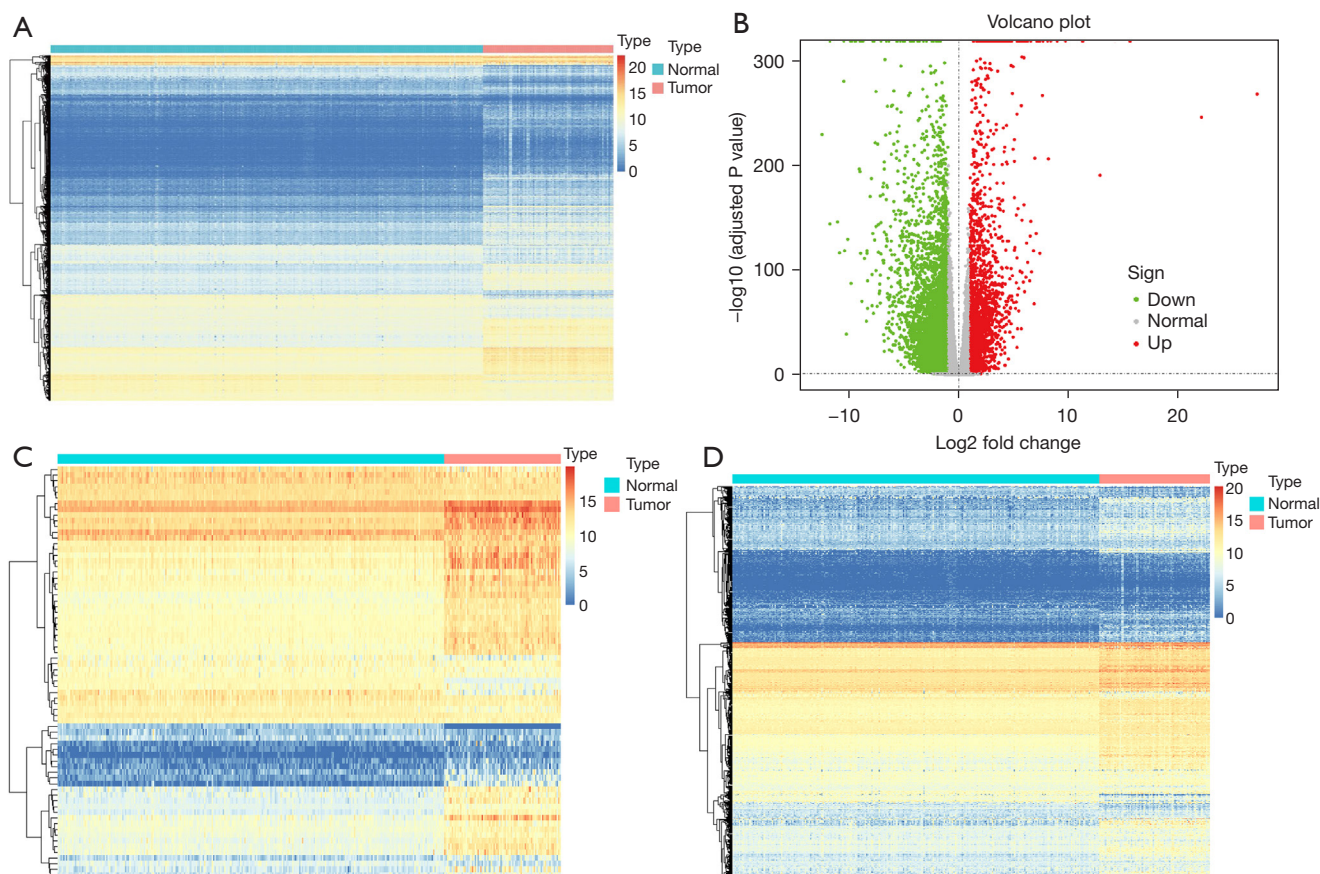


Figure 1 Differentially expressed hypoxia-related genes (DEHRGs) and differentially expressed immune-related genes (DEIRGs) in patients with esophageal squamous cell carcinoma (ESCC). Heat map (A) and volcano plot (B) of differentially expressed genes (DEGs) in ESCC and normal esophageal tissues. Heat map of DEHRGs (C) and DEIRGs (D) in ESCC and normal esophageal tissues.

Functional enrichment analysis of DEIRGs and DEHRGs

The biological functions of DEIRGs and DEHRGs were investigated using GO annotation and KEGG pathway analyses. Several hypoxia-related GO terms were identified, such as “small molecule metabolic process”, “extracellular region”, and “transferase activity” (Figure 2A-2C). The most significant hypoxia-related KEGG term was “HIF-1 signaling pathway” (Figure 2D). Several immune-related GO terms were identified, such as “response to chemical”, “extracellular region”, and “signaling receptor binding” (Figure 2E-2G). The most significant immune-related KEGG term was “cytokine-cytokine receptor interaction” (Figure 2H).

Development of the risk score signature and assessment of its predictive ability

To identified hypoxia- and immune-related prognostic DEGs, 73 DEHRGs and 548 DEIRGs were screened using univariate Cox regression analyses. We obtained 3 DEHRGs genes and 8 DEIRGs genes with significantly effects on patient prognosis, respectively. The results of the Cox analysis are illustrated by forest plots (Figure 3A). Using the LASSO method, a total of 10 genes were obtained by combining 2 sets of factors. Redundant factors were removed, 8 related factors were retained, and a prognostic risk score model was constructed according to the expression values of the 8 factors (Figure 3B-3E). By using

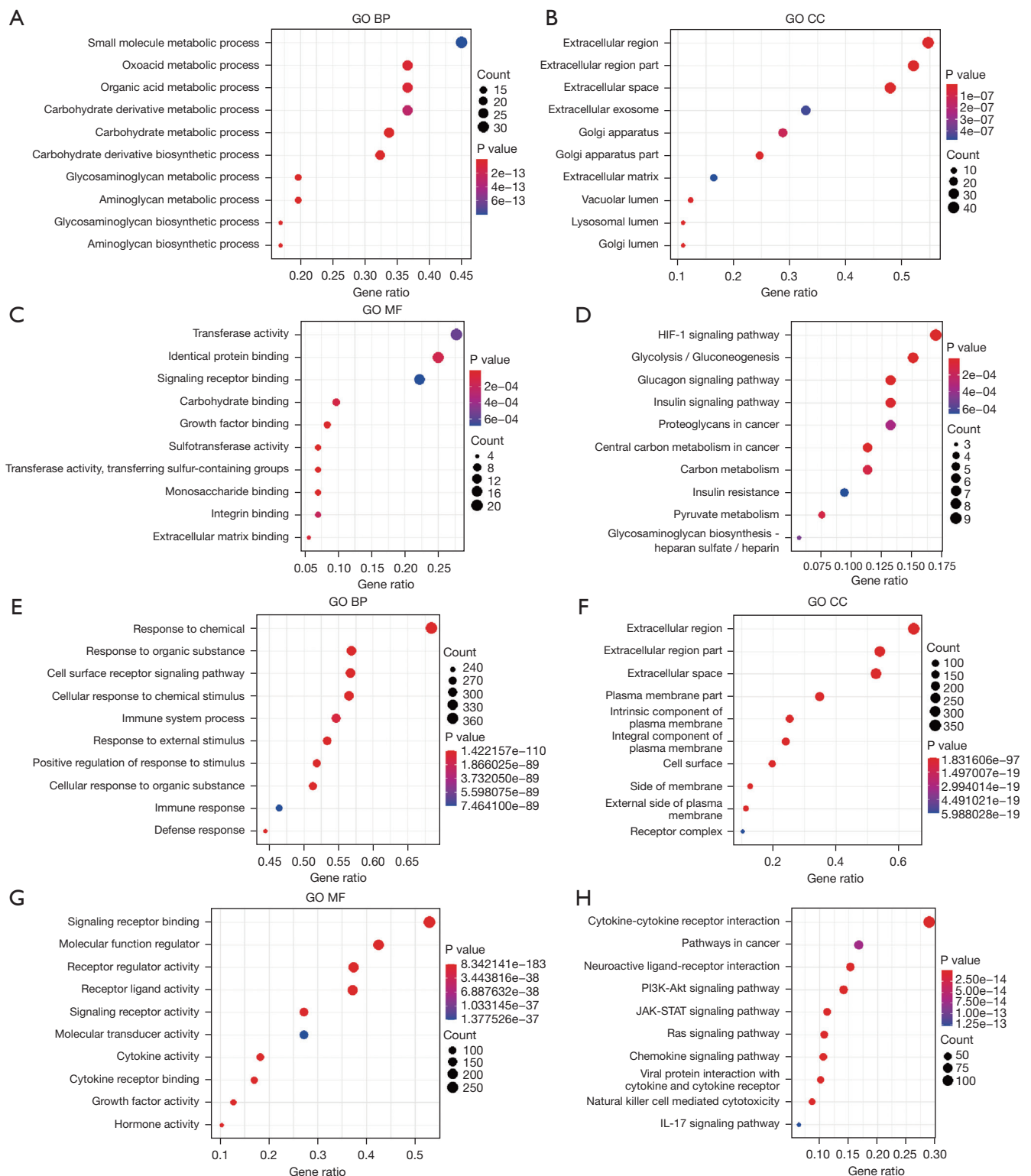


Figure 2 Functional enrichment analysis of differentially expressed hypoxia-related genes (DEHRGs) and differentially expressed immunerelated genes (DEIRGs). (A-C) Functional enrichment of Gene Ontology (GO) terms of DEHRGs; (D) functional enrichment of Kyoto Encyclopedia of Genes and Genomes (KEGG) terms of DEHRGs; (E-G) functional enrichment of GO terms of DEIRGs; (H) functional enrichment of KEGG terms of DEIRGs.

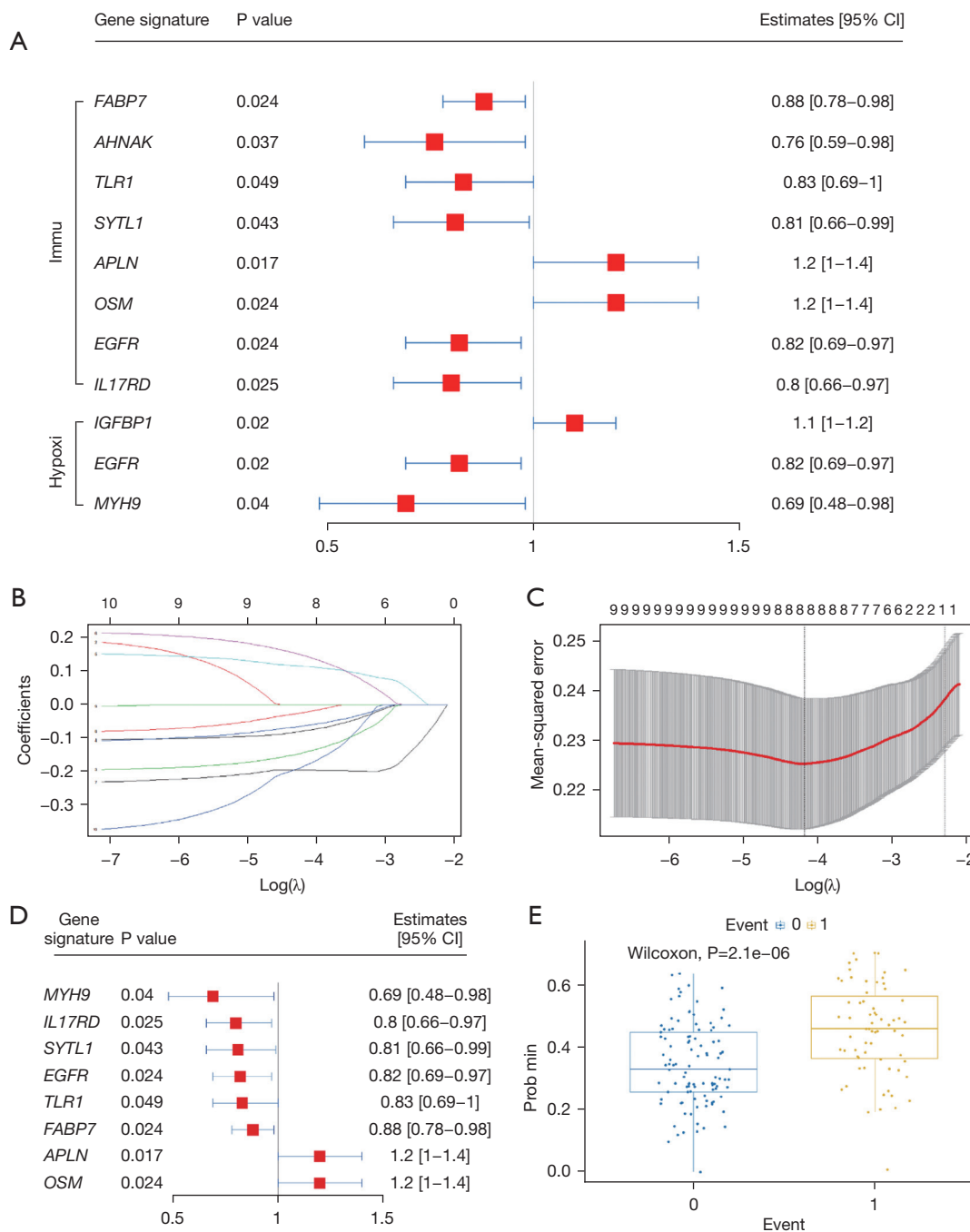


Figure 3 Hypoxia- and immune-associated prognosis signature. (A) Forest plot of hazard ratios for 10 hypoxia- and immune-associated prognostic differentially expressed genes (DEGs). (B) Least absolute shrinkage and selection operator (LASSO) coefficient profiles of the hypoxia- and immune-associated prognostic DEGs. Each curve in the figure represents the changing trajectory of each independent variable coefficient. The Y axis indicates the value of the coefficient. The lower X axis shows $\log(\lambda)$ and the upper X axis shows the number of non-zero coefficients in the model. (C) Three-fold cross-validation of the tuning parameter selection in the LASSO model. The lower X axis indicates $\log(\lambda)$, and the upper X axis indicates the average number of genes associated with prognosis. Partial likelihood deviance values are shown, with error bars representing standard error (SE). The vertical black dotted lines are drawn at the optimal values by minimum criteria and $1 - SE$ criteria, which provides the best fit; (D) Forest plot of hazard ratios for 8 hypoxia- and immune-associated prognostic DEGs; (E) Distributions of risk score and survival status. The predicted value of event 1 (death) is significantly higher than event 0 (survival).

the Cox regression model, the risk score of each patient was calculated as follows: risk score = $(-0.079 \times \text{expression of } FABP7) + (-0.143 \times \text{expression of } TLR1) + (-0.063 \times \text{expression of } SYTL1) + (0.115 \times \text{expression of } APLN) + (0.146 \times \text{expression of } OSM) + (-0.196 \times \text{expression of } EGFR) + (-0.023 \times \text{expression of } IL17RD) + (-0.183 \times \text{expression of } MYH9)$. Based on this 8-gene-based risk score, a risk prognosis classifier was constructed to classify the samples into high- and low-risk groups according to the median risk score (Figure 4A). Survival curves of high- and low-risk samples were plotted (Figure 4B), which showed that the survival rate of high-risk samples was significantly lower than that of low-risk samples. The risk curve and signature DEG expression patterns are plotted in Figure 4C. In this model, the AUC was 0.715, suggesting that the model could be used for predicting survival (Figure 4D). Heat map of the expression distribution of 8 genes in the model was shown in Figure 4E.

Risk model stability analysis

To determine model stability, the survival curve was plotted based on known clinical variables (including smoking, BMI, radiotherapy, TMN staging, and sex). The clinicopathological characteristics of patients divided into the low- and high-risk groups are listed in Table 1. The risk score model of the 8 clinical variables, such as N0, N1, M0, and male, showed significant intergroup differences (high- and low-risk grouping) in these clinical characteristics, indicating that the predictive efficiency and stability of the model were favorable (Figure 5).

Relationship between the risk score model and immune cell infiltration

As the tumors of the high-risk group were proven to be infiltrated with a large number of immune cells, we further analyzed the correlation between risk score and subtypes of infiltrating immune cells. The results indicated that the levels of infiltrating resting dendritic cells and naïve CD4⁺ T cells in the high-risk group were lower than those of the low-risk group ($P < 0.05$, Figure 6A-6D). In contrast, the levels of infiltrating activated mast cells, Tregs, and neutrophils in the high-risk group were higher than those of the low-risk group ($P < 0.05$, Figure 6E-6F). Consequently, the high-risk group had abundant immunosuppressive cells, resulting in an immunosuppressive TME, which corresponds to poor prognosis.

Nomogram model can predict the OS probability of ESCC

The nomogram model was constructed to predict the OS of ESCC patients at 1, 2, and 3 years by integrating the risk score and well-known prognostic factors, including age, BMI, histological grade, and tumor TNM staging information (Figure 7A). The calibration curve approached the ideal curve (black straight line) in the calibration diagram, indicating that the predicted OS probability was compatible with the actual probability (Figure 7B).

Discussion

Considering the significant differences between the prognoses of ESCC patients, it is crucial to develop a reliable, convenient, and cost-effective prognostic signature to maximize the benefits of personalized treatment and for guiding prognosis. The present study has important guiding value for determining the prognosis of ESCC patients based on gene information obtained from ESCC samples in this study.

Previous studies have indicated that long non-coding RNA (lncRNA) signatures could be used as prognostic tools for patients with ESCC (17,18). Nevertheless, the application of lncRNAs is limited due to their technical specifications and expensive testing costs. A recent study identified an immune-related risk signature to predict the outcome of ESCC patients (19). However, the heterogeneity of the tumor immune microenvironment and tumor hypoxia were not considered in the research. In this study, the comprehensive mining of hypoxia- and immune-associated genes was used to construct a model to aid in prognosis prediction. We identified a series of HRGs and IRGs associated with prognosis in ESCC patients. Moreover, a hypoxia- and immune-associated signature composed of 8 genes was developed as a prognostic classification tool with promising effectiveness and stability. Finally, the nomogram model was constructed to predict the OS of ESCC patients, demonstrating favorable prediction ability.

Hypoxia is a strong aggravator of ESCC progression. It can accelerate tumor glycolysis, angiogenesis, cell proliferation, metastasis, and radio- and chemo-resistance (5,20). Hypoxia, or hypoxic tension, has become one of the hallmarks of the TME (21). Rapid tumor growth requires a large amount of nutrients and oxygen supply, which triggers tumor angiogenesis. However, tumor angiogenesis is highly abnormal and inefficient. Oxygenation of the perivascular tumor area depends on the diffusion gradient relative to the

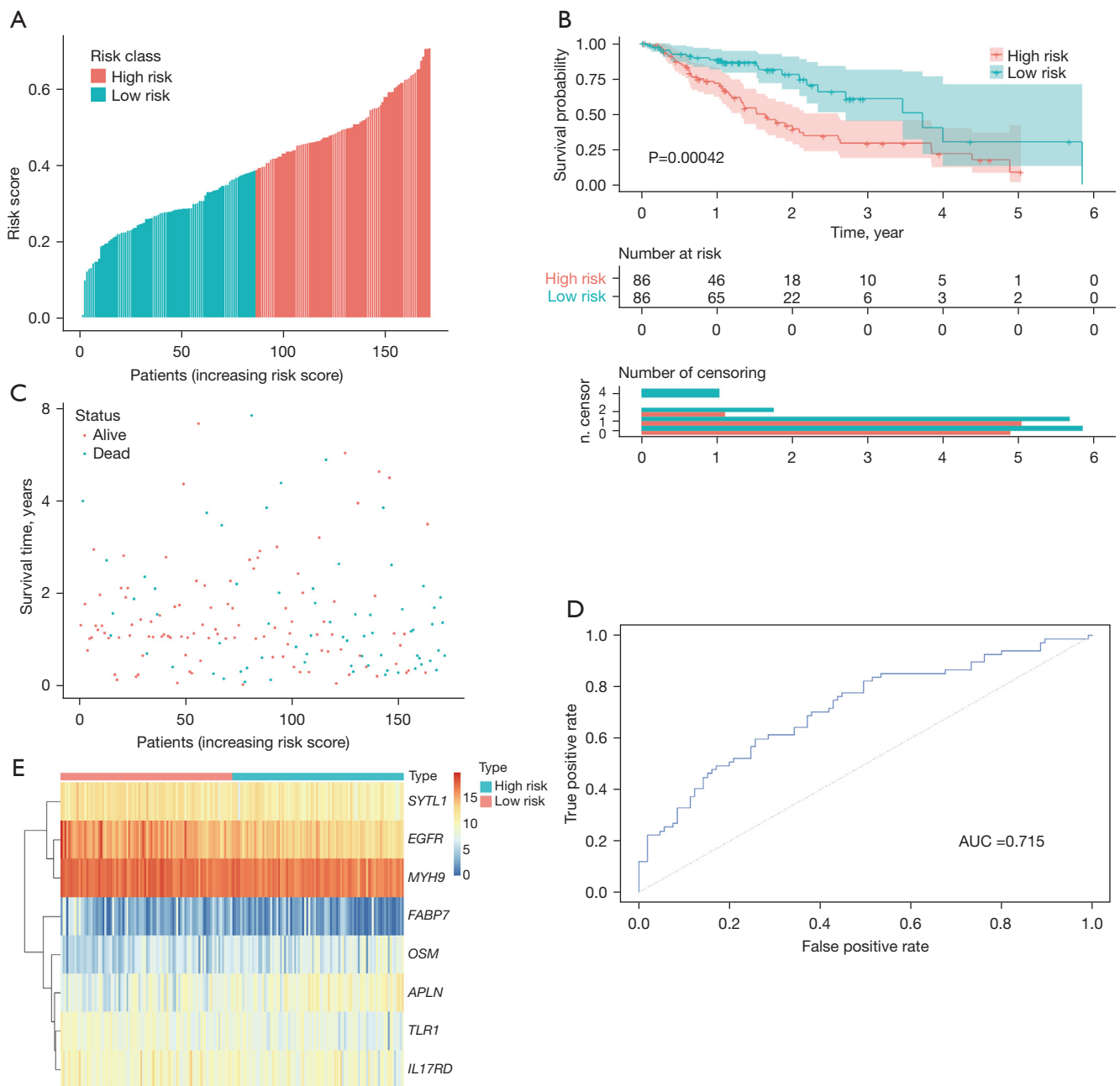


Figure 4 Validation of the effectiveness of the hypoxia- and immune-associated prognosis prediction model. (A) The high- and low-risk groups according to the median risk score; (B) Kaplan-Meier curves of overall survival (OS) in 172 patients of the training cohort based on risk score; (C) distributions of risk score and survival status; (D) survival-dependent receiver operating characteristic (ROC) curve validation of the model for prognosis; (E) heat map of the expression distribution of 8 genes in the prognosis model. Red indicates high expression and blue indicates low expression.

intravascular oxygen partial pressure (PO₂), which leads to hypoxia in remote areas (22,23). Studies have confirmed the existence of tumor hypoxia in ESCC, and hypoxia is

considered to be a key risk factor of poor prognosis in ESCC patients (23,24).

Furthermore, hypoxia can promote and maintain

Table 1 The clinicopathologic characteristics of patients with esophageal squamous cell carcinoma

Characteristic	Low risk (%)	High risk (%)	P value
Age			0.479
≤65 years	50 (79.4)	10 (66.7)	
>65 years	13 (20.6)	5 (33.3)	
Sex			0.878
Female	9 (14.3)	3 (20.0)	
Male	54 (85.7)	12 (80.0)	
Pathologic M			0.667
M0	57 (90.5)	14 (93.3)	
M1	3 (4.8)	0 (0)	
MX	3 (4.8)	1 (6.7)	
Pathologic N			0.189
N0	35 (55.6)	10 (66.7)	
N1	22 (34.9)	4 (26.7)	
N2	5 (7.9)	0 (0)	
N3	0 (0)	1 (6.7)	
NX	1 (1.6)	0 (0)	
Pathologic T			0.009
T1	7 (11.1)	1 (6.7)	
T2	18 (28.6)	9 (60.0)	
T3	37 (58.7)	3 (20.0)	
T4	1 (1.6)	2 (13.3)	
Neoplasm histologic grade			0.029
G1	9 (14.3)	6 (40.0)	
G2	35 (55.6)	3 (20.0)	
G3	14 (22.2)	3 (20.0)	
Missing	5 (7.9)	3 (20.0)	
Radiation therapy			0.115
Not reported	13 (20.6)	7 (46.7)	
No	30 (47.6)	5 (33.3)	
Yes	20 (31.7)	3 (20.0)	
BMI exposures			0.403
≤24	45 (71.4)	9 (60.0)	
>24	15 (23.8)	6 (40.0)	
Missing	3 (4.8)	0 (0)	

Table 1 (continued)**Table 1** (continued)

Characteristic	Low risk (%)	High risk (%)	P value
Cigarettes per day exposures			1.000
≤1	9 (14.3)	3 (20.0)	
>1	27 (42.9)	7 (46.7)	
Missing	27 (42.9)	5 (33.3)	
Alcohol history exposures			0.392
No	17 (27.0)	2 (13.3)	
Not reported	2 (3.2)	0 (0)	
Yes	44 (69.8)	13 (86.7)	

an immunosuppressive TME (25). Hypoxia mediates immunosuppression mainly by restraining T cell migration into tumor tissue or accelerating T cell apoptosis (26). Besides, hypoxia drives immune evasion through the up-regulation of HIF-1 α secretion (27).

In the present study, we found that hypoxia and immune status were correlated with the prognosis of ESCC. The HRGs *MYH9* and *EGFR* were associated with ESCC prognosis, while the IRGs *FABP7*, *TLR1*, *SYTL1*, *APLN*, *OSM*, *EGFR*, and *IL17RD* were associated with ESCC prognosis. Furthermore, a correlation was also observed between hypoxia, immune status, and survival information. Therefore, these HRGs and IRGs deserve further investigation.

The important roles of the characteristic genes identified in this study have been reported in a variety of cancer types including ESCC. Myosin heavy chain 9 (*MYH9*) deletion inhibits glycolysis, migration, and invasion of gastric cancer cells in the hypoxic TME (28). *MYH9* is a novel mutant gene in ESCC. The expression of *MYH9* was significantly up-regulated in ESCC, and was associated with lymph node metastasis in ESCC patients. Moreover, down-regulation of *MYH9* gene expression can inhibit cell migration, invasion, and gene expression changes related to angiogenesis and epithelial-mesenchymal transition (EMT) (29). In addition, as the substrate of protein tyrosine phosphatase 1B (*PTP1B*), *MYH9* can be dephosphorylated by *PTP1B*, thereby up-regulating the expression of epidermal growth factor receptor (*EGFR*) and enhancing cell migration and invasion in ESCC (30). *EGFR* is a key molecule in the pathophysiology of ESCC and is highly expressed on the surface of ESCC cells (31). Genetic variants in *EGFR* are associated with the prognosis of ESCC patients after

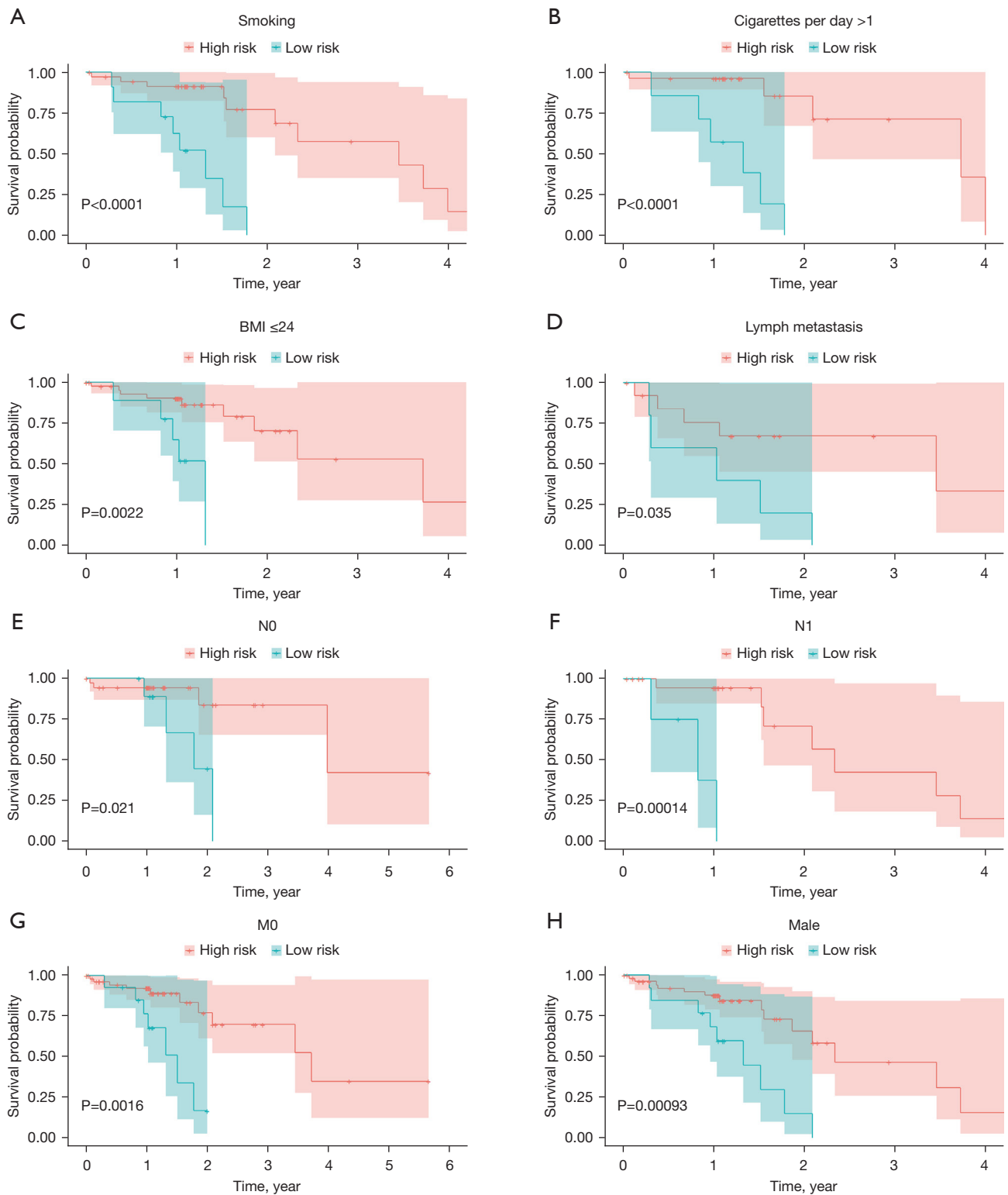
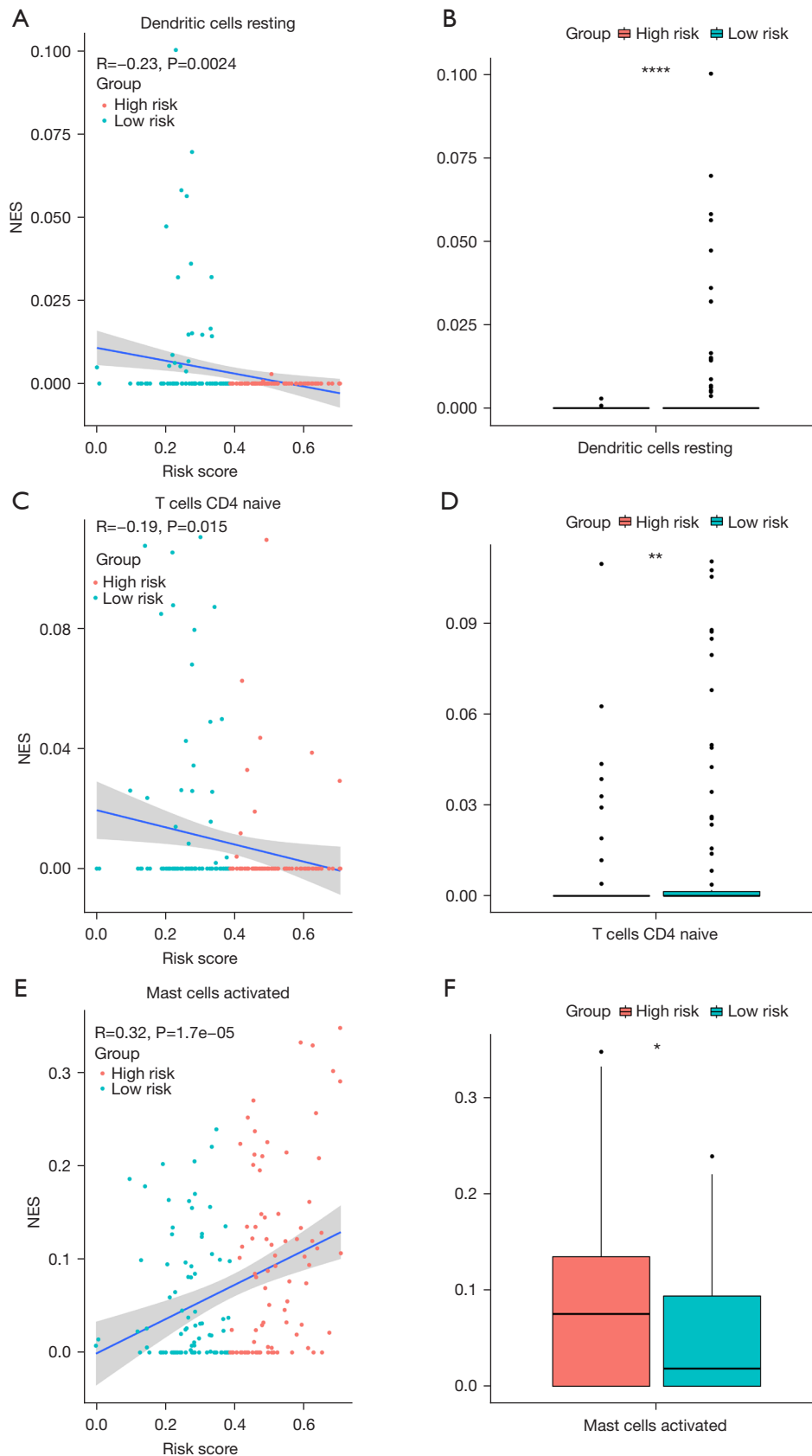


Figure 5 Validation of the stability of the hypoxia- and immune-associated prognosis prediction model. Kaplan-Meier plot of overall survival by risk groups according to smoking status (A); more than 1 cigarette per day (B); body mass index (BMI) ≤ 24 kg/m² (C); patients who received radiotherapy (D); N0 staging (E); N1 staging (F); M0 staging (G); and male gender (H).



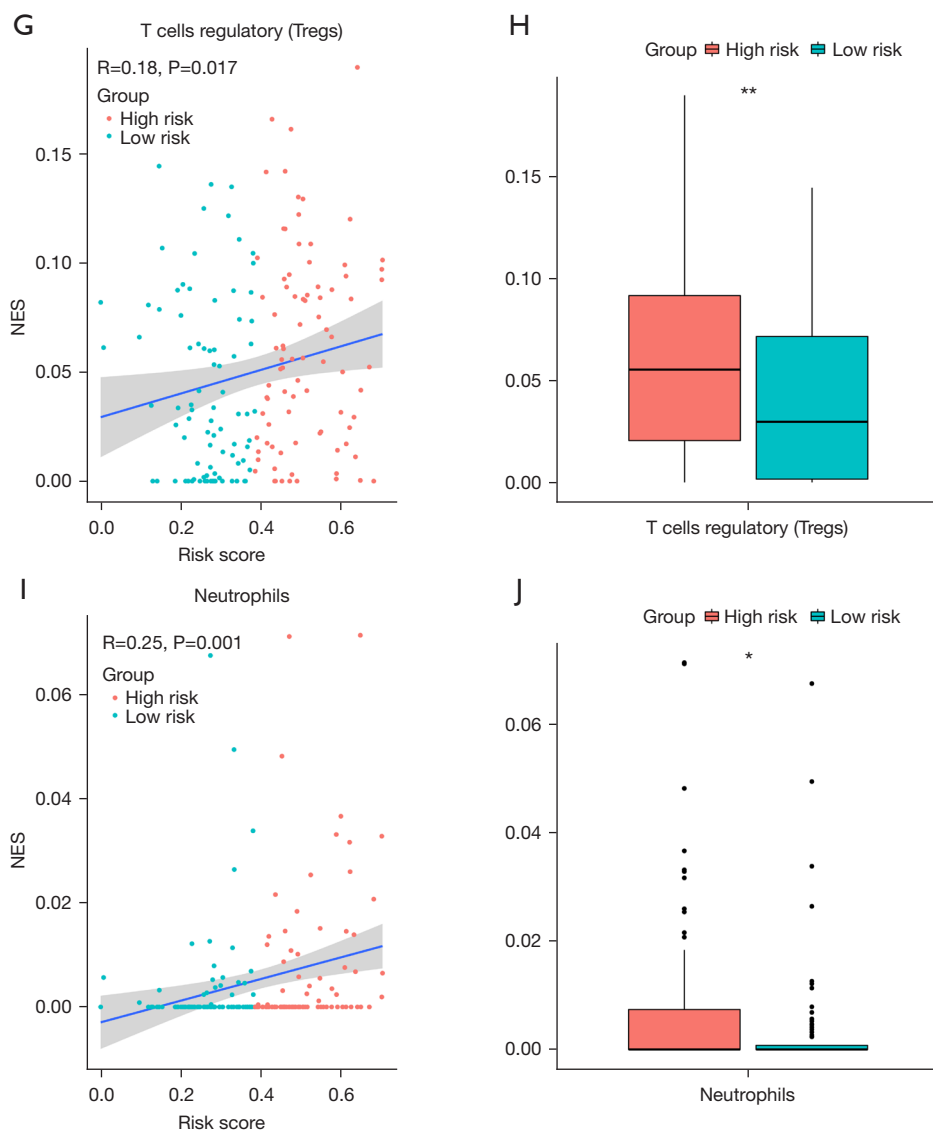


Figure 6 Relationship between the risk score and immune cell infiltration. (A,B) Resting dendritic cells; (C,D) naive CD4⁺ T cells; (E,F) activated mast cells; (G,H) regulatory T cells; (I,J) neutrophils. *P<0.05, **P<0.01, and ****P<0.0001. NES, normalized enrichment score.

radical resection (32). Oncostatin M (*OSM*) regulates tumor infiltration of immune cells and is associated with the outcome of cholangiocarcinoma (33). The expression of *OSM* is up-regulated in hepatocellular carcinoma (HCC) (34). *OSM* induces tumor necrosis factor- α (TNF- α) secretion and CD68⁺ macrophage aggregation. In addition, the expression of *OSM* is correlated with a low OS rate in HCC (34). Apelin (*APLN*) is abnormally up-regulated in HCC and is correlated with poor outcome (35). Inhibition of *APLN* can potentially remodel the TME, reduce angiogenesis, and effectively inhibit tumor growth.

Moreover, up-regulation of *APLN* was associated with poor outcome (36). Interleukin-17 receptor D (*IL17RD*), an immune-related gene, is correlated with the outcome of cervical squamous cell carcinoma (37), muscle-invasive bladder cancer (38), and medullary thyroid cancer (39). Synaptotagmin-like 1 (*SYTL1*), also known as *Slp1*, promotes leukemogenesis and facilitates the interaction between leukemic cells and bone marrow stroma (40). The up-regulation of toll-like receptor 1 (*TLR1*) is associated with better outcomes of pancreatic ductal adenocarcinoma (PDAC) patients (41). *TLR1* is highly expressed in breast

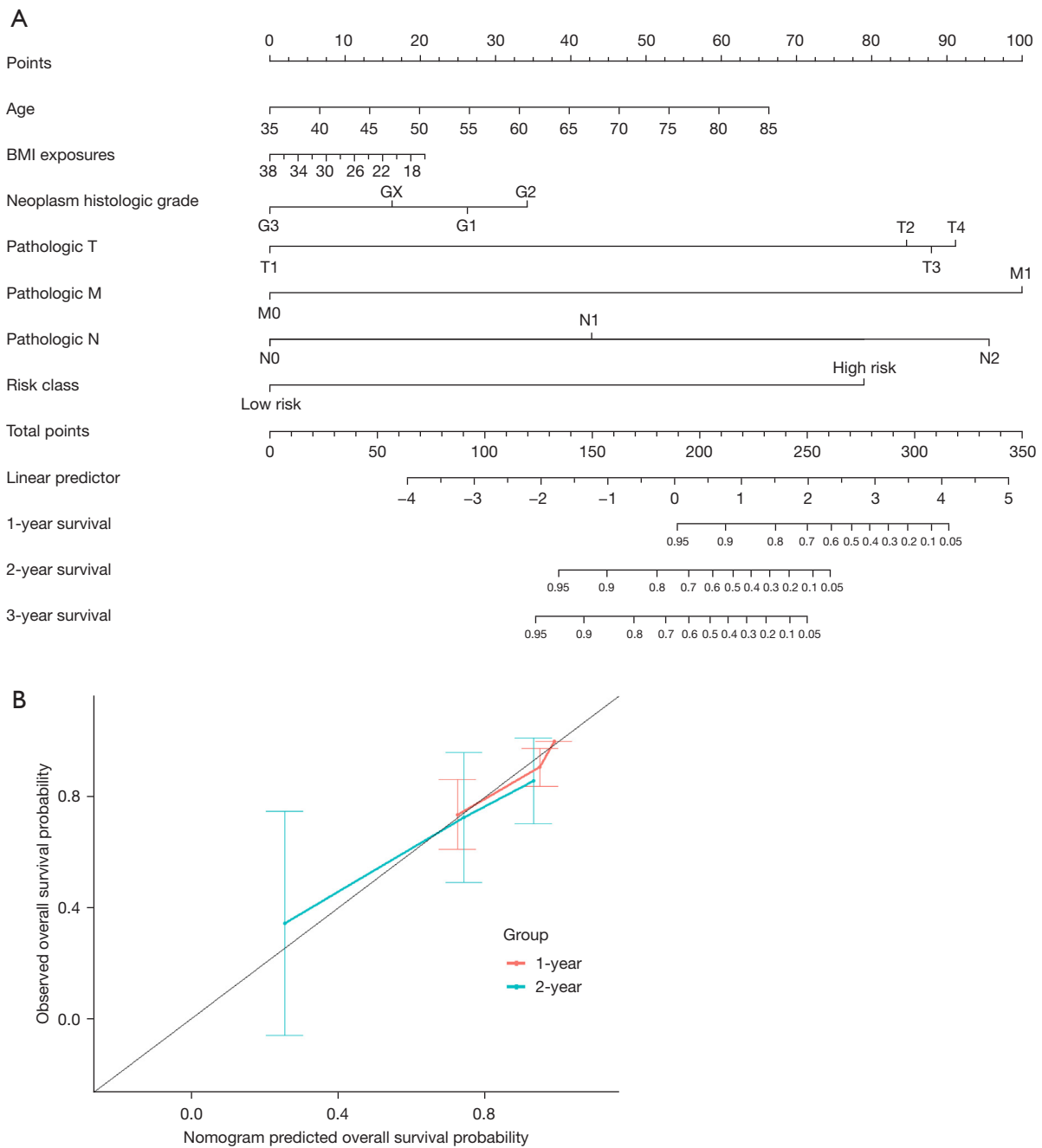


Figure 7 Development and evaluation of the nomogram for predicting overall survival. (A) Nomogram based on the risk score and clinicopathological characteristics to predict the 1-, 2-, and 3-year overall survival probability. Calibration of the nomogram according to the consistency between the predicted and the actual results. (B) The nomogram depicts curves relative to the black line, suggesting perfect prediction.

cancer and may serve as a biomarker of its pathogenesis and progression (42). A high level of fatty acid binding protein 7 (*FABP7*) is correlated with poor prognosis in several types

of malignant tumors (43). A recent study demonstrated that *FABP7* was a favorable biomarker for predicting better response to neoadjuvant chemotherapy (NAC) in breast

cancer patients (44).

Immune cell infiltration is a key factor affecting tumor progression and prognosis. In recent years, a series of researchers have reported that immune cell infiltration could provide promising signatures for the prognostic prediction of colon cancer (45) and lung adenocarcinoma (46). In this study, we found higher infiltration of Tregs, activated mast cells, and neutrophils in the high-risk group based on our model. Zhang *et al.* have also reported higher infiltration of Tregs in high-risk patients, which was consistent with our results (19). These findings suggest that high-risk patients are more likely to present with negative immunomodulatory infiltrating cells. Meanwhile, our data contributes to the understanding of immune status of different risk groups, which will be helpful for clinical practice.

However, there were several limitations in our research. First, we included approximately 200 HRGs and 1,793 IRGs in the present study, which might not be sufficient for a comprehensive analysis. Second, tumor hypoxia and immunosuppressive TME were considered to be highly heterogeneous. Considering the characteristics of the tumor, the composition varies according to the location and time of tumor progression, and the predictive ability of our 8-gene hypoxia- and immune-associated signature might vary according to different regions of tumor tissue. Lastly, this research lacked a large cohort and longer follow-up for further validation. Thus, the hypoxia- and immune-associated signature constructed in this study requires further validation by more prospective, multicenter studies.

Conclusions

In conclusion, the present study identified a series of hypoxia- and immune-related genes associated with the prognosis of ESCC patients. Furthermore, we established a practicable and reproducible hypoxia- and immune-associated risk signature for ESCC and revealed new information related to the hypoxia and immune status of ESCC. Ultimately, a nomogram model was constructed to predict the OS of ESCC which demonstrated favorable prediction ability. We believe that our model may contribute to individualized management, follow-up plans, and treatment strategies for ESCC patients.

Acknowledgments

Funding: This work was supported by The Science

and Technology Project Foundation of Suzhou (Nos. SS201852, SS202093, and SYSD2020061); the Science and Education for Health Foundation of Suzhou for Youth (No. KJXW2019074); and the Youth Medical Science and Technology Innovation Project of Xuzhou Health Committee (No. XWKYHT20200024).

Footnote

Reporting Checklist: The authors have completed the TRIPOD reporting checklist. Available at <https://jgo.amegroups.com/article/view/10.21037/jgo-22-69/rc>

Conflicts of Interest: All authors have completed the ICMJE uniform disclosure form (available at <https://jgo.amegroups.com/article/view/10.21037/jgo-22-69/coif>). The authors have no conflicts of interest to declare.

Ethical Statement: The authors are accountable for all aspects of the work in ensuring that questions related to the accuracy or integrity of any part of the work are appropriately investigated and resolved. The study was conducted in accordance the Helsinki Declaration (as revised in 2013). All data in this article is obtained from the public database.

Open Access Statement: This is an Open Access article distributed in accordance with the Creative Commons Attribution-NonCommercial-NoDerivs 4.0 International License (CC BY-NC-ND 4.0), which permits the non-commercial replication and distribution of the article with the strict proviso that no changes or edits are made and the original work is properly cited (including links to both the formal publication through the relevant DOI and the license). See: <https://creativecommons.org/licenses/by-nc-nd/4.0/>.

References

1. Bray F, Ferlay J, Soerjomataram I, et al. Global cancer statistics 2018: GLOBOCAN estimates of incidence and mortality worldwide for 36 cancers in 185 countries. *CA Cancer J Clin* 2018;68:394-424.
2. Baba Y, Yoshida N, Kinoshita K, et al. Clinical and Prognostic Features of Patients With Esophageal Cancer and Multiple Primary Cancers: A Retrospective Single-institution Study. *Ann Surg* 2018;267:478-83.
3. Rustgi AK, El-Serag HB. Esophageal carcinoma. *N Engl J Med* 2014;371:2499-509.

4. Mao Y, Wang Y, Dong L, et al. Hypoxic exosomes facilitate angiogenesis and metastasis in esophageal squamous cell carcinoma through altering the phenotype and transcriptome of endothelial cells. *J Exp Clin Cancer Res* 2019;38:389.
5. Zhang Q, Zhang J, Fu Z, et al. Hypoxia-induced microRNA-10b-3p promotes esophageal squamous cell carcinoma growth and metastasis by targeting TSGA10. *Aging (Albany NY)* 2019;11:10374-84.
6. Shao N, Han Y, Song L, et al. Clinical significance of hypoxia-inducible factor 1 α , and its correlation with p53 and vascular endothelial growth factor expression in resectable esophageal squamous cell carcinoma. *J Cancer Res Ther* 2020;16:269-75.
7. Lin W, Wu S, Chen X, et al. Characterization of Hypoxia Signature to Evaluate the Tumor Immune Microenvironment and Predict Prognosis in Glioma Groups. *Front Oncol* 2020;10:796.
8. Baba Y, Nomoto D, Okadome K, et al. Tumor immune microenvironment and immune checkpoint inhibitors in esophageal squamous cell carcinoma. *Cancer Sci* 2020;111:3132-41.
9. Zheng Y, Chen Z, Han Y, et al. Immune suppressive landscape in the human esophageal squamous cell carcinoma microenvironment. *Nat Commun* 2020;11:6268.
10. Maghsudlu M, Farashahi Yazd E. Heat-induced inflammation and its role in esophageal cancer. *J Dig Dis* 2017;18:431-44.
11. Chang WH, Lai AG. The pan-cancer mutational landscape of the PPAR pathway reveals universal patterns of dysregulated metabolism and interactions with tumor immunity and hypoxia. *Ann N Y Acad Sci* 2019;1448:65-82.
12. Tan L, Cheng D, Wen J, et al. Identification of prognostic hypoxia-related genes signature on the tumor microenvironment in esophageal cancer. *Math Biosci Eng* 2021;18:7743-58.
13. Tibshirani R. The lasso method for variable selection in the Cox model. *Stat Med* 1997;16:385-95.
14. Newman AM, Liu CL, Green MR, et al. Robust enumeration of cell subsets from tissue expression profiles. *Nat Methods* 2015;12:453-7.
15. Iasonos A, Schrag D, Raj GV, et al. How to build and interpret a nomogram for cancer prognosis. *J Clin Oncol* 2008;26:1364-70.
16. Heagerty PJ, Lumley T, Pepe MS. Time-dependent ROC curves for censored survival data and a diagnostic marker. *Biometrics* 2000;56:337-44.
17. Li W, Liu J, Zhao H. Identification of a nomogram based on long non-coding RNA to improve prognosis prediction of esophageal squamous cell carcinoma. *Aging (Albany NY)* 2020;12:1512-26.
18. Zhang L, Li P, Liu E, et al. Prognostic value of a five-lncRNA signature in esophageal squamous cell carcinoma. *Cancer Cell Int* 2020;20:386.
19. Zhang C, Luo Y, Zhang Z, et al. Identification of a Prognostic Immune Signature for Esophageal Squamous Cell Carcinoma to Predict Survival and Inflammatory Landscapes. *Front Cell Dev Biol* 2020;8:580005.
20. Zhang H, Si J, Yue J, et al. The mechanisms and reversal strategies of tumor radioresistance in esophageal squamous cell carcinoma. *J Cancer Res Clin Oncol* 2021;147:1275-86.
21. Buckley AM, Lynam-Lennon N, O'Neill H, et al. Targeting hallmarks of cancer to enhance radiosensitivity in gastrointestinal cancers. *Nat Rev Gastroenterol Hepatol* 2020;17:298-313.
22. Horsman MR, Mortensen LS, Petersen JB, et al. Imaging hypoxia to improve radiotherapy outcome. *Nat Rev Clin Oncol* 2012;9:674-87.
23. Peerlings J, Van De Voorde L, Mitea C, et al. Hypoxia and hypoxia response-associated molecular markers in esophageal cancer: A systematic review. *Methods* 2017;130:51-62.
24. Jing X, Yang F, Shao C, et al. Role of hypoxia in cancer therapy by regulating the tumor microenvironment. *Mol Cancer* 2019;18:157.
25. Chang CH, Qiu J, O'Sullivan D, et al. Metabolic Competition in the Tumor Microenvironment Is a Driver of Cancer Progression. *Cell* 2015;162:1229-41.
26. Joyce JA, Fearon DT. T cell exclusion, immune privilege, and the tumor microenvironment. *Science* 2015;348:74-80.
27. Vito A, El-Sayes N, Mossman K. Hypoxia-Driven Immune Escape in the Tumor Microenvironment. *Cells* 2020;9:992.
28. Fang X, Bai Y, Zhang L, et al. Silencing circSLAMF6 represses cell glycolysis, migration, and invasion by regulating the miR-204-5p/MYH9 axis in gastric cancer under hypoxia. *Biosci Rep* 2020;40:BSR20201275.
29. Yang B, Liu H, Bi Y, et al. MYH9 promotes cell metastasis via inducing Angiogenesis and Epithelial Mesenchymal Transition in Esophageal Squamous Cell Carcinoma. *Int J Med Sci* 2020;17:2013-23.
30. Pan BQ, Xie ZH, Hao JJ, et al. PTP1B up-regulates EGFR expression by dephosphorylating MYH9 at Y1408 to promote cell migration and invasion in esophageal squamous cell carcinoma. *Biochem Biophys Res Commun* 2020;522:53-60.

31. Kikuchi O, Ohashi S, Horibe T, et al. Novel EGFR-targeted strategy with hybrid peptide against oesophageal squamous cell carcinoma. *Sci Rep* 2016;6:22452.
32. Wang YL, Yuan Y, Luo XX, et al. Genetic Variants in EGFR/PLCE1 Pathway Are Associated with Prognosis of Esophageal Squamous Cell Carcinoma after Radical Resection. *Curr Med Sci* 2019;39:385-90.
33. Liu Q, Lan T, Song Y, et al. Oncostatin M expression and TP53 mutation status regulate tumor-infiltration of immune cells and survival outcomes in cholangiocarcinoma. *Aging (Albany NY)* 2020;12:21518-43.
34. Yang X, Shao C, Duan L, et al. Oncostatin M promotes hepatic progenitor cell activation and hepatocarcinogenesis via macrophage-derived tumor necrosis factor- α . *Cancer Lett* 2021;517:46-54.
35. Chen H, Wong CC, Liu D, et al. APLN promotes hepatocellular carcinoma through activating PI3K/Akt pathway and is a druggable target. *Theranostics* 2019;9:5246-60.
36. Uribealago I, Hoffmann D, Zhang Y, et al. Apelin inhibition prevents resistance and metastasis associated with anti-angiogenic therapy. *EMBO Mol Med* 2019;11:e9266.
37. Wang Q, Vattai A, Vilsmaier T, et al. Immunogenomic Identification for Predicting the Prognosis of Cervical Cancer Patients. *Int J Mol Sci* 2021;22:2442.
38. Jin K, Qiu S, Jin D, et al. Development of prognostic signature based on immune-related genes in muscle-invasive bladder cancer: bioinformatics analysis of TCGA database. *Aging (Albany NY)* 2021;13:1859-71.
39. Chang YS, Chang CC, Huang HY, et al. Detection of Molecular Alterations in Taiwanese Patients with Medullary Thyroid Cancer Using Whole-Exome Sequencing. *Endocr Pathol* 2018;29:324-31.
40. Yokoyama T, Nakatake M, Kuwata T, et al. MEIS1-mediated transactivation of synaptotagmin-like 1 promotes CXCL12/CXCR4 signaling and leukemogenesis. *J Clin Invest* 2016;126:1664-78.
41. Lanki M, Seppänen H, Mustonen H, et al. Toll-like receptor 1 predicts favorable prognosis in pancreatic cancer. *PLoS One* 2019;14:e0219245.
42. Shi S, Xu C, Fang X, et al. Expression profile of Toll-like receptors in human breast cancer. *Mol Med Rep* 2020;21:786-94.
43. Kagawa Y, Umaru BA, Ariful I, et al. Role of FABP7 in tumor cell signaling. *Adv Biol Regul* 2019;71:206-18.
44. Xie Q, Xiao YS, Jia SC, et al. FABP7 is a potential biomarker to predict response to neoadjuvant chemotherapy for breast cancer. *Cancer Cell Int* 2020;20:562.
45. Zhou R, Zhang J, Zeng D, et al. Immune cell infiltration as a biomarker for the diagnosis and prognosis of stage I-III colon cancer. *Cancer Immunol Immunother* 2019;68:433-42.
46. Zuo S, Wei M, Wang S, et al. Pan-Cancer Analysis of Immune Cell Infiltration Identifies a Prognostic Immune-Cell Characteristic Score (ICCS) in Lung Adenocarcinoma. *Front Immunol* 2020;11:1218.

(English Language Editor: C. Betlazar-Maseh)

Cite this article as: Lian L, Teng SB, Xia YY, Shen XM, Zheng Y, Han SG, Wang WJ, Xu XF, Zhou C. Development and verification of a hypoxia- and immune-associated prognosis signature for esophageal squamous cell carcinoma. *J Gastrointest Oncol* 2022;13(2):462-477. doi: 10.21037/jgo-22-69

Table S1 Hypoxia-related genes list

PGK1
 PDK1
 GBE1
 PFKL
 ALDOA
 ENO2
 PGM1
 NDRG1
 HK2
 ALDOC
 GPI
 MXI1
 SLC2A1
 P4HA1
 ADM
 P4HA2
 ENO1
 PFKP
 AK4
 FAM162A
 PFKFB3
 VEGFA
 BNIP3L
 TPI1
 ERO1A
 KDM3A
 CCNG2
 LDHA
 GYS1
 GAPDH
 BHLHE40
 ANGPTL4
 JUN
 SERPINE1
 LOX
 GCK

Table S1 (continued)

Table S1 (continued)

PPFIA4
 MAFF
 DDIT4
 SLC2A3
 IGFBP3
 NFIL3
 FOS
 RBPJ
 HK1
 CITED2
 ISG20
 GALK1
 WSB1
 PYGM
 STC1
 ZNF292
 BTG1
 PLIN2
 CSRP2
 VLDLR
 JMJD6
 EXT1
 F3
 PDK3
 ANKZF1
 UGP2
 ALDOB
 STC2
 ERRF1
 ENO3
 PNRC1
 HMOX1
 PGF
 GAPDHS
 CHST2
 TMEM45A

Table S1 (continued)

Table S1 (continued)

BCAN
ATF3
CAV1
AMPD3
GPC3
NDST1
IRS2
SAP30
GAA
SDC4
STBD1
IER3
PKLR
IGFBP1
PLAUR
CAVIN3
CCN5
LARGE1
NOCT
S100A4
RRAGD
ZFP36
EGFR
EDN2
IDS
CDKN1A
RORA
DUSP1
MIF
PPP1R3C
DPYSL4
KDEL3
DTNA
ADORA2B
HS3ST1
CAVIN1

Table S1 (continued)**Table S1** (continued)

NR3C1
KLF6
GPC4
CCN1
TNFAIP3
CA12
HEXA
BGN
PPP1R15A
PGM2
PIM1
PRDX5
NAGK
CDKN1B
BRS3
TKTL1
MT1E
ATP7A
MT2A
SDC3
TIPARP
PKP1
ANXA2
PGAM2
DDIT3
PRKCA
SLC37A4
CXCR4
EFNA3
CP
KLF7
CCN2
CHST3
TPD52
LXN
B4GALNT2

Table S1 (continued)

Table S1 (*continued*)

PPARGC1A
BCL2
GCNT2
HAS1
KLHL24
SCARB1
SLC25A1
SDC2
CASP6
VHL
FOXO3
PDGFB
B3GALT6
SLC2A5
SRPX
EFNA1
GLRX
ACKR3
PAM
TGFB1
DCN
SIAH2
PLAC8
FBP1
TPST2
PHKG1
MYH9
CDKN1C
GRHPR
PCK1
INHA
HSPA5
NDST2
NEDD4L
TPBG

Table S1 (*continued*)**Table S1** (*continued*)

XPNPEP1
IL6
SLC6A6
MAP3K1
LDHC
AKAP12
TES
KIF5A
LALBA
COL5A1
GPC1
HDLBP
ILVBL
NCAN
TGM2
ETS1
HOXB9
SELENBP1
FOSL2
SULT2B1
TGFB3
